LETTER

doi:10.1038/nature14306

Niche-induced cell death and epithelial phagocytosis regulate hair follicle stem cell pool

Kailin R. Mesa[1], Panteleimon Rompolas[1], Giovanni Zito[2], Peggy Myung[1,3], Thomas Y. Sun[1], Samara Brown[1], David G. Gonzalez[4], Krastan B. Blagoev[5,6], Ann M. Haberman[4] & Valentina Greco[1,3,7,8]

Tissue homeostasis is achieved through a balance of cell production (growth) and elimination (regression)[1,2]. In contrast to tissue growth, the cells and molecular signals required for tissue regression remain unknown. To investigate physiological tissue regression, we use the mouse hair follicle, which cycles stereotypically between phases of growth and regression while maintaining a pool of stem cells to perpetuate tissue regeneration[3]. Here we show by intravital microscopy in live mice[4–6] that the regression phase eliminates the majority of the epithelial cells by two distinct mechanisms: terminal differentiation of suprabasal cells and a spatial gradient of apoptosis of basal cells. Furthermore, we demonstrate that basal epithelial cells collectively act as phagocytes to clear dying epithelial neighbours. Through cellular and genetic ablation we show that epithelial cell death is extrinsically induced through transforming growth factor (TGF)-β activation and mesenchymal crosstalk. Strikingly, our data show that regression acts to reduce the stem cell pool, as inhibition of regression results in excess basal epithelial cells with regenerative abilities. This study identifies the cellular behaviours and molecular mechanisms of regression that counterbalance growth to maintain tissue homeostasis.

Tissue regression in the hair follicle is thought to be mediated through programmed cell death[7]. However, it is unclear which cells within the follicle are removed and whether this process is a result of intrinsic cellular exhaustion or active elimination by extrinsic factors. We used our established intravital microscopy technique[4] to visualize cell behaviours non-invasively in live mice during hair follicle regression (Fig. 1a, Extended Data Fig. 1 and Supplementary Video 1). Unexpectedly, time-lapse recordings of epithelial nuclei (made visible using H2B–green fluorescent protein (GFP) driven by the keratin 14 promoter (*K14-H2BGFP*)) revealed a lack of cell death by nuclear fragmentation in the suprabasal (inner) layers. Furthermore, time-lapse recordings and genetic lineage-tracing approaches showed that inner layers were eliminated through upward terminal differentiation[8] (Fig. 1b, c, Extended Data Fig. 2 and Supplementary Video 2).

In contrast, using live imaging we captured cell death in the basal epithelial layer. Furthermore, we found that apoptotic debris was retained within the basal epithelium and relocated around neighbouring nuclei, suggesting that basal epithelial cells may act as phagocytes to remove epithelial cellular debris during hair follicle regression (Fig. 1d and Supplementary Video 3). To test this, we induced mosaic expression of a cytoplasmic tdTomato fluorescent reporter in the basal layer. This showed internalization of tdTomato$^+$ epithelial debris into neighbouring tdTomato$^-$ basal epithelial cells (Fig. 1e). Ultrastructure analysis confirmed phagocytosis of apoptotic bodies by basal epithelial cells (Fig. 1f and Extended Data Fig. 3). Tracking this process in real time with cytoskeletal and nuclear labelling demonstrated that apoptotic debris from a single cell was dispersed within the surrounding epithelium and collectively internalized by neighbouring basal epithelial cells (Fig. 1g and Supplementary Videos 4–6). Consistent with these findings, professional phagocytes[9] were neither present inside the regressing hair follicles nor did they colocalize with epithelial cell debris (Extended Data Fig. 4 and Supplementary Videos 7, 8). Taken together, these data reveal two modes of epithelial cell elimination during hair follicle regression. While suprabasal cells undergo terminal differentiation, basal epithelial cells undergo apoptosis and are collectively removed by their basal epithelial neighbours. These findings, along with work done on the mammary gland[10,11], support a new paradigm of physiological epithelial self-clearance.

Thus far, we have demonstrated that the basal epithelium adopts new cellular behaviours from growth to regression[4,5]. During growth, highly mitotic cells fuel downwards extension of the basal epithelium. These basal cells, located in the lower follicle, are also more likely to be eliminated during regression, suggesting a model in which mitotic exhaustion primes cells for death[12]. An alternative model could be that cell death is driven by extrinsic cues based on spatial location in the basal epithelium. To test these models, we promoted survival intrinsically in the basal epithelium using the Wnt/β-catenin signalling pathway, which is expressed in the suprabasal layers and has been implicated in survival of these cells[13] (Fig. 2a and Extended Data Fig. 5). We used a Cre-inducible genetic model to activate β-catenin signalling ectopically in single cells of the basal epithelium[6] and track survival during regression *in vivo* (Fig. 2b). Control experiments confirmed a spatial bias of cell survival in the upper basal layer, as suggested by previous work[12]. Although β-catenin activation was observed to enhance cell survival throughout the follicle, the spatial bias of cell survival seen in controls was retained in the β-catenin-activated follicles (Fig. 2c, d). These data suggest that cell intrinsic factors such as Wnt/β-catenin signalling alone do not explain the pattern of cell survival observed and implicate extrinsic factors to induce cell death in the basal epithelium.

These results prompted us to ask whether the observed pattern of basal cell survival was the result of spatially regulated induction of cell death. Quantifications of cell death events in time-lapse recordings of various stages of regression revealed an initial localized induction of cell death at the bottom of the follicle, which is in direct contact with the hair follicle mesenchymal dermal papilla niche (Fig. 3a and Supplementary Video 9). Therefore, we hypothesized that interaction with the dermal papilla promotes cell death along the basal epithelium of the hair follicle. To test this, we used two-photon laser ablation[4] specifically to remove the dermal papilla at the onset of regression and revisited the same hair follicles over time (Fig. 3b). Dermal papilla ablation resulted in significantly reduced death of basal epithelial cells as measured by hair follicle length when compared to neighbouring unablated hair follicles (Fig. 3c and Extended Data Fig. 6). Significant differences in ablated and unablated hair follicle lengths are seen as early as 2 days after ablation, suggesting that the dermal papilla directly promotes regression (Fig. 3d). The difference in length of ablated and unablated hair follicles could be

[1]Department of Genetics, Yale School of Medicine, New Haven, Connecticut 06510, USA. [2]Department of Biopathology and Medical Biotechnology, University of Palermo, via Divisi 83, 90100 Palermo, Italy. [3]Department of Dermatology, Yale School of Medicine, New Haven, Connecticut 06510, USA. [4]Department of Laboratory Medicine, Department of Immunobiology, Yale School of Medicine, New Haven, Connecticut 06510, USA. [5]National Science Foundation, Arlington, Virginia 22230, USA. [6]AA Martinos Center for Biomedical Imaging, Department of Radiology, Massachusetts General Hospital, Harvard Medical School, Boston, Massachusetts 02114, USA. [7]Yale Stem Cell Center, Yale School of Medicine, New Haven, Connecticut 06510, USA. [8]Yale Cancer Center, Yale School of Medicine, New Haven, Connecticut 06510, USA.

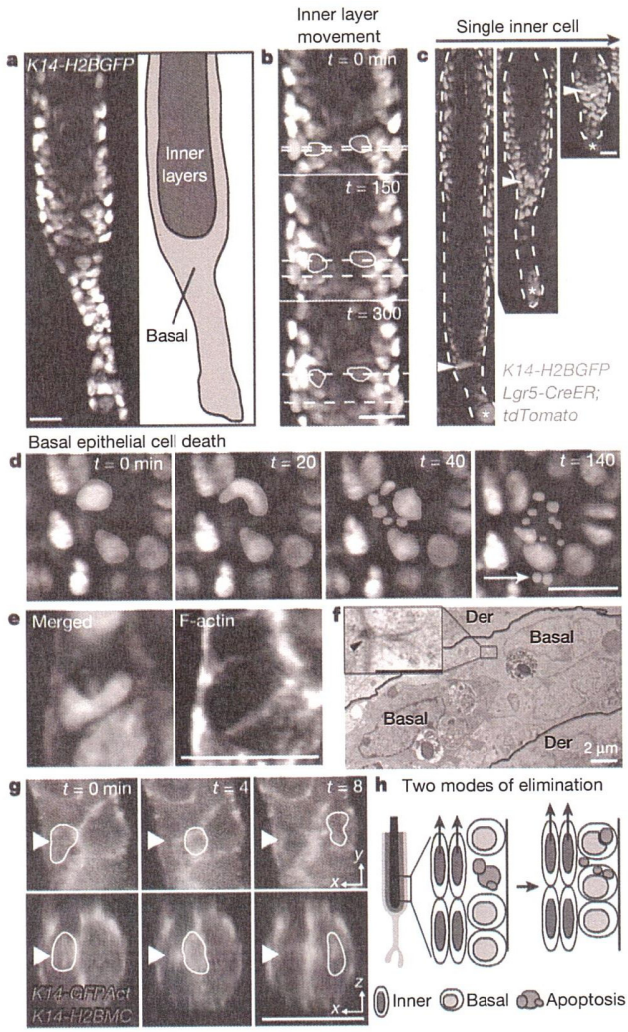

Figure 1 | Basal epithelial cells collectively act as phagocytes to clear neighbouring epithelial cell debris. **a**, Schematic of hair follicle in regression, indicating the basal and suprabasal (inner) epithelial layers, using *K14-H2BGFP* mice. **b**, Single optical sections showing upward collective movement of inner layers in relation to surrounding basal epithelial cells at successive time points, 2.5 h apart (compare position of yellow and white dashed lines). **c**, Single-cell lineage tracing of inner layer cells during regression ($n = 30$ cells, in 4 mice). Labelled cells were revisited daily. Asterisk indicates mesenchymal dermal papilla. **d**, Single optical sections showing cell death (nuclear fragmentation) at successive time points. Note that fragments (green) relocate (white arrow) around neighbouring epithelial nuclei (yellow, red and blue). **e**, Whole-mount staining showing engulfment of neighbouring basal epithelial cellular content by phalloidin staining (blue) in with mosaic Cre induction in basal layer. Nucleus is indicated in green and cytoplasm in red. **f**, Electron micrograph illustrating multiple apoptotic bodies (red arrowhead) present in basal epithelial cells. Basal, basal epithelial cell; Der, dermis. Inset shows high-magnification electron micrograph depicting desmosomal junctions (arrowhead) of phagocytic epithelial cells. Scale bar, 500 nm. **g**, Single optical sections of both coronal and transverse planes (x,y and x,z) at successive time points 4 min apart showing internalization of an apoptotic body (yellow border) by a neighbouring basal epithelial cell. Nucleus is indicated in red and cell cortex in green. **h**, Scheme of the two modes of elimination of epithelial cells and collective phagocytic uptake of basal epithelial apoptotic bodies by neighbouring basal epithelial cells during regression. Scale bars, 20 μm unless otherwise indicated.

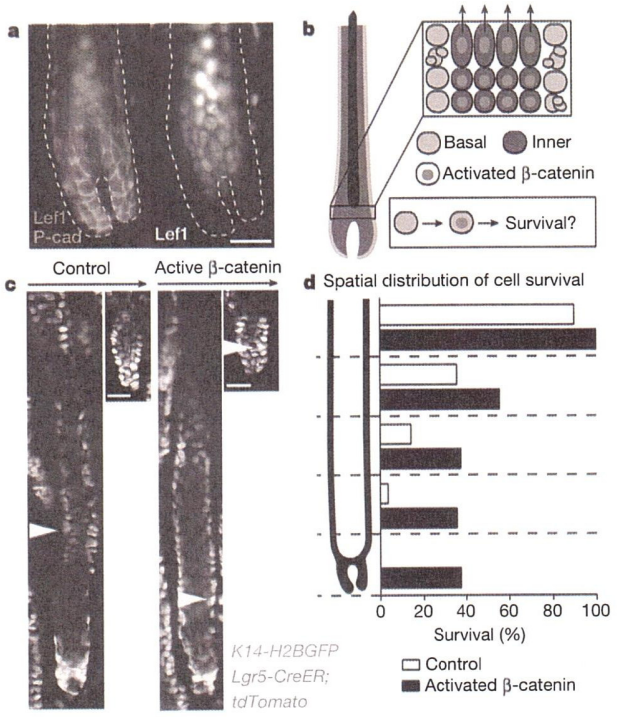

Figure 2 | β-catenin activation is not sufficient to overcome the extrinsic gradient of basal epithelial survival. **a**, Wnt/β-catenin activation is restricted to inner layers. Immunofluorescent staining of Lef1 in regressing hair follicle. Lef1 is indicated in red and P-cadherin (P-cad) in green. **b**, Scheme of basal and inner layer behaviours and β-catenin activation during hair follicle regression. **c**, Lineage tracing of basal epithelial cells revisited at the beginning and end of regression. Representative examples of either a single control or β-catenin-activated cell traced during regression. **d**, Graphical representation of cell survival as a function of initial position within the regressing hair follicle ($n = 235$ or 135 in control or β-catenin, respectively, in 4 mice). Scale bars, 25 μm.

attributed to a reduction in cell death or a reduction in cell clearance. To be able to distinguish the effect of the dermal papilla on these two processes, we quantified the number of apoptotic debris sites in ablated follicles 2 days after ablation and found that the amount of cellular debris was significantly reduced compared to control follicles at this initial time point. The debris generated from these follicles by day 2 was cleared by day 4, similar to control follicles, suggesting that cell clearance is relatively unaffected by dermal papilla removal (Fig. 3e). Collectively, this establishes a functional role for the mesenchymal niche to promote basal epithelial cell death.

To understand the molecular signalling that facilitates basal epithelial cell death, we investigated the TGF-β signalling pathway, as exogenous administration of TGF-β1 ligand has been shown to induce precocious hair follicle regression[14]. We found that TGF-β ligands are expressed by the mesenchymal dermal papilla, whereas TGF-β signalling is active in the basal epithelium during the regression phase (Fig. 3f–h and Extended Data Figs 7, 8a). To test the functional role of TGF-β signalling in basal epithelial cell death during regression, we conditionally eliminated TGF-β receptor 1 (TGF-βR1) in the basal layer[15] (Extended Data Fig. 8b, c). Removal of TGF-βR1 at the onset of regression resulted in aberrant accumulation of basal cells by the end of regression when compared to control littermates (Fig. 3i–k). Together, these data demonstrate that extrinsic regulation through TGF-β signalling and epithelial–mesenchymal crosstalk induces cell death along the basal epithelium while sparing a restricted pool of stem cells.

This work raises the question of whether hair follicle regression serves to eliminate either exhausted basal cells or functional cells from an expanded stem cell pool. To address this question, we used an approach to remove the dermal papilla transiently[16] during regression (Fig. 4a). Strikingly, as neighbouring unablated follicles began a new round of growth, dermal-papilla-ablated follicles that had failed to complete

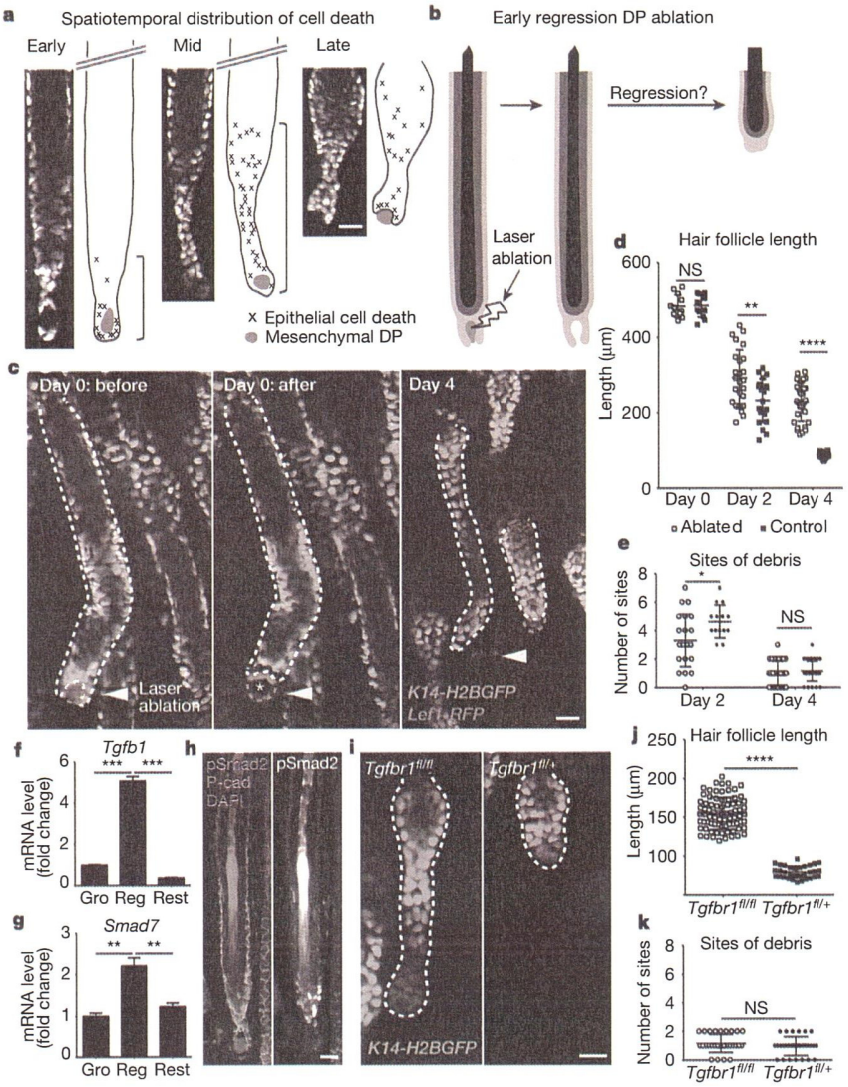

Figure 3 | Mesenchymal dermal papilla crosstalk and TGF-β signalling are required for cell death in the basal epithelium. **a**, Graphical representation and quantification of spatial distribution of cell death in the basal layer at three stages of regression using time-lapse recordings ($n = 9$ follicles, in 5 mice). DP, dermal papilla. **b**, Scheme of laser ablation experiment. **c**, Sequential revisits of hair follicles after dermal papilla ablation during regression. Yellow arrowhead indicates laser ablation site. Asterisk indicates auto-fluorescence from the two-photon laser. **d**, **e**, Dot plot quantification of the hair follicle length at day 0, 2 and 4 after dermal papilla ablation (**d**) and of the number of apoptotic fragmentation sites at day 2 and 4 after dermal papilla ablation (**e**) ($n = 36$ follicles, in 6 mice; mean ± standard deviation (s.d.)). **f**, **g**, Messenger RNA levels of *Tgfb1* ligand expression in the mesenchymal dermal papilla (**f**) and *Smad7* expression in hair follicle basal layer throughout the hair cycle (**g**) (mean ± s.d.; $n = 3$ technical replicates). Hair follicle phases indicated as: Gro, growth; Reg, regression; Rest. **h**, Localized TGF-β activation by immunofluorescent staining of phosphorylated (p)Smad2 at the onset of hair follicle regression. 4′,6-Diamidino-2-phenylindole (DAPI), blue; pSmad2, red; P-cadherin, green. **i**, Hair follicles after Cre-induced recombination in $Tgfbr1^{fl/fl}$ and $Tgfbr1^{fl/+}$ mice at the end of regression. **j**, **k**, Dot plot quantification of the hair follicle length (**j**) and of the number of apoptotic fragmentation sites at the end of regression (**k**) ($n = 31$ follicles, in 4 mice; mean ± s.d.). NS, not significant. $^{*}P < 0.05$, $^{**}P < 0.01$, $^{***}P < 0.001$ and $^{****}P < 0.0001$ indicate a significant difference. Scale bars, 25 μm.

regression also initiated hair growth from the bottom of their aberrantly long basal epithelium. Furthermore, ablated hair follicles appeared grossly normal, with proper generation of differentiated suprabasal layers, similar to neighbouring unablated hair follicles (Fig. 4b). These findings demonstrate that basal epithelial cells of the hair follicle are not intrinsically committed for cell death, but rather retain a capacity to regenerate tissue. This suggests that regression functions to reduce an expanded stem cell pool following tissue growth.

We show that physiological regression is an extrinsically regulated process that reduces the size of the hair follicle stem cell compartment

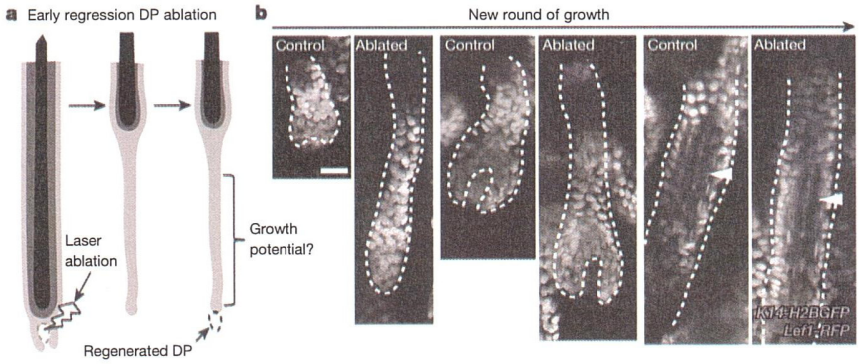

Figure 4 | Basal epithelial cells targeted for cell death retain regenerative potential. **a**, Scheme of laser ablation experiment. **b**, Sequential revisits of hair follicles after dermal papilla (DP) ablation during the next round of growth (postnatal day (P)22–P35). White arrowhead indicates differentiated inner layers. Observations shown represent $n = 3$ mice. Scale bars, 25 μm.

while leaving terminal differentiation programs unaffected. Regression is regulated through TGF-β signalling initiated by the mesenchymal niche to induce spatially restricted cell death in the basal epithelium. Clearance of apoptotic cells is a self-contained process driven by epithelial phagocytosis within the regressing basal epithelium. Finally, inhibition of regression through transient loss of the mesenchymal niche demonstrates that cells throughout the hair follicle basal epithelium maintain regenerative competency when in proximity to the mesenchymal niche (Extended Data Fig. 9). All together, we demonstrate that tissue regression relies on spatially coordinated cellular behaviours, and establish a new understanding of the extrinsic regulation that counterbalances tissue growth over the lifespan of an organism.

Online Content Methods, along with any additional Extended Data display items and Source Data, are available in the online version of the paper; references unique to these sections appear only in the online paper.

Received 19 July 2014; accepted 9 February 2015.
Published online 6 April 2015.

1. Bergmann, A. & Steller, H. Apoptosis, stem cells, and tissue regeneration. *Sci. Signal.* **3,** re8 (2010).
2. Poon, I. K., Lucas, C. D., Rossi, A. G. & Ravichandran, K. S. Apoptotic cell clearance: basic biology and therapeutic potential. *Nature Rev. Immunol.* (2014).
3. Müller-Röver, S. *et al.* A comprehensive guide for the accurate classification of murine hair follicles in distinct hair cycle stages. *J. Invest. Dermatol.* **117,** 3–15 (2001).
4. Rompolas, P. *et al.* Live imaging of stem cell and progeny behaviour in physiological hair-follicle regeneration. *Nature* **487,** 496–499 (2012).
5. Rompolas, P., Mesa, K. R. & Greco, V. Spatial organization within a niche as a determinant of stem-cell fate. *Nature* (2013).
6. Deschene, E. R. *et al.* β-Catenin Activation Regulates Tissue Growth Non–Cell Autonomously in the Hair Stem Cell Niche. *Science* **343,** 1353–1356 (2014).
7. Lindner, G. *et al.* Analysis of apoptosis during hair follicle regression (catagen). *Am. J. Pathol.* **151,** 1601 (1997).
8. Rogers, G. E. Hair follicle differentiation and regulation. *Int. J. Dev. Biol.* **48,** 163–170 (2004).
9. Li, J. L. *et al.* Intravital multiphoton imaging of immune responses in the mouse ear skin. *Nature Protocols* **7,** 221–234 (2012).
10. Monks, J. *et al.* Epithelial cells as phagocytes: apoptotic epithelial cells are engulfed by mammary alveolar epithelial cells and repress inflammatory mediator release. *Cell Death Differ.* **12,** 107–114 (2005).
11. Monks, J., Smith-Steinhart, C., Kruk, E. R., Fadok, V. A. & Henson, P. M. Epithelial cells remove apoptotic epithelial cells during post-lactation involution of the mouse mammary gland. *Biol. Reprod.* **78,** 586–594 (2008).
12. Hsu, Y.-C., Pasolli, H. A. & Fuchs, E. Dynamics between stem cells, niche, and progeny in the hair follicle. *Cell* **144,** 92–105 (2011).
13. Choi, Y. S. *et al.* Distinct functions for Wnt/β-catenin in hair follicle stem cell proliferation and survival and interfollicular epidermal homeostasis. *Cell Stem Cell* **13,** 720–733 (2013).
14. Foitzik, K. *et al.* Control of murine hair follicle regression (catagen) by TGF-β1 *in vivo*. *FASEB J.* **14,** 752–760 (2000).
15. Larsson, J. *et al.* TGF-β signalling-deficient hematopoietic stem cells have normal self-renewal and regenerative ability *in vivo* despite increased proliferative capacity *in vitro*. *Blood* **102,** 3129–3135 (2003).
16. Rahmani, W. *et al.* Hair follicle mesenchymal stem cells regenerate the dermal sheath, replenish the dermal papilla and specify hair type. *Dev. Cell* **31,** 543–558 (2014).

Supplementary Information is available in the online version of the paper.

Acknowledgements We thank E. Fuchs for the *K14-H2BGFP*, *Lef1-RFP* and *K14-GFPActin* mice; M. Taketo for the *Cttnb1*$^{fl(Ex3)/+}$ mice; A. Horwich and A. Mesa for critical feedback; M. Rendl for technical advice; M. Graham and X. Liu for technical support with electron microscopy; D. Egli for the H2BmCherry construct; and T. Nottoli for generating the *K14-H2BmCherry* mouse line. K.R.M. and S.B. were supported by the National Institutes of Health (NIH) Predoctoral Program in Cellular and Molecular Biology, grant no. 5T32 GM007223. K.R.M. is currently a National Science Foundation (NSF) Graduate Research Fellow. This work is supported by the American Cancer Society, grant no. RSG-12-059-02; Yale Spore Grant National Cancer Institute, NIH, grant no. 2P50CA121974; the National Institute of Arthritis and Musculoskeletal and Skin Diseases (NIAMS), NIH, grant no. 1R01AR063663-01; and by The New York Stem Cell Foundation. V.G. is a New York Stem Cell Foundation–Robertson Investigator. P.R. is a New York Stem Cell Foundation–Druckenmiller Fellow. A.M.H. is supported by NIAMS Rheumatic Diseases Research Core Centers grant no. 5 P30 AR053495-07. K.B.B. was supported by the NSF. The NSF had no role in study design, data collection and analysis, decision to publish, or preparation of the manuscript. The views presented here are not those of the NSF and represent solely the views of the authors.

Author Contributions K.R.M. and V.G. designed experiments and wrote the manuscript; K.R.M. performed the experiments and analysed the data. P.R. generated the *K14-H2BmCherry* mouse line and assisted with two-photon time-lapse imaging. G.Z. and P.M. performed immunofluorescence. S.B. performed skin whole-mount staining. T.Y.S. assisted with technical aspects. K.R.M., D.G.G. and A.M.H. performed three-dimensional imaging analysis. K.B.B. helped with data analysis.

Author Information Reprints and permissions information is available at www.nature.com/reprints. The authors declare no competing financial interests. Readers are welcome to comment on the online version of the paper. Correspondence and requests for materials should be addressed to V.G. (valentina.greco@yale.edu).

METHODS

Mice. *K14-H2BGFP*[17], *Lef1-RFP*[18] and *K14-GFPActin*[19] were obtained from the Fuchs Laboratory. *Tgfbr1*$^{fl/fl}$ mice were obtained from V. Kaartinen[15]. *Ctnnb1*$^{fl(Ex3)/+}$ mice were obtained from M. Taketo[20]. *Lgr5-CreER* (Clevers Laboratory), *Shh-CreER* (Tabin Laboratory), *LysM-Cre* (Foerster Laboratory), *Cx3cr1-GFP* (Littman Laboratory) and *Rosa-stop-tdTomato* (Zeng Laboratory) were obtained from Jackson Laboratory (JAX)[21–25]. The Yale Transgenic Facility generated the *K14-H2BmCherry* mice. All studies and procedures involving animal subjects were approved by the Institutional Animal Care and Use Committee at Yale School of Medicine and conducted in accordance with the approved animal handling protocol. *Lgr5-CreER* and *Shh-CreER* were used to recombine alleles and label cells conditionally within specific hair follicle populations and temporally during the regression phase. Cre induction for the lineage-tracing experiments was induced with a single intraperitoneal injection of tamoxifen (1 μg g^{-1} in corn oil) at postnatal day 14. *Tgfbr1*$^{fl/fl}$ recombination was induced with three intraperitoneal injections of tamoxifen (100 μg g^{-1} in corn oil) at postnatal day 10, 12 and 14. Intravital microscopy and laser ablation procedures were carried out as described previously[4,5]. For lineage-tracing experiments, only cells that were unambiguously separated from neighbouring cells were sampled to ensure the identity of individual lineages. Mice from experimental and control groups were randomly selected of either gender for live imaging experiments. No blinding was done. All lineage-tracing and ablation experiments were repeated in at least three different mice.

Generation of *K14H2BmCherry* mice. Transgenic mice expressing H2BmCherry under the control of the keratin 14 promoter (*K14-H2BmCherry*) were generated using the following procedure. The H2BmCherry insert (provided by D. Egli) was amplified by PCR from the TopoTA vector (Life Technologies) using primers 5′-CGGCGGATCCATGCCAGAGCCAGC and 3′-CGCTCTAGATTACTTGTACAGCTCGTCC, which introduced cleavage sites for BamHI and XbaI restriction enzymes immediately upstream and downstream, respectively, of the open reading frame. The 1.1 kb PCR product was inserted between the BamHI and XbaI sites in the pG3Z*K14cassette vector (provided by E. Fuchs). The resulting transgene was digested with SacI and SphI, and the 4.3 kb fragment was injected into blastocysts at the Yale Transgenic Facility (T. Nottoli). Chimaeric mice were screened initially by PCR and founder mice were selected to establish transgenic mouse lines. These initial lines were subsequently screened by histological analysis, and the line displaying the highest expression levels of the K14H2BmCherry reporter was selected to establish the final colony.

***In vivo* imaging and laser ablation.** Mice between postnatal day 17 and 35 were anaesthetized with intraperitoneal injection of 7 μl g^{-1} of ketamine/xylazine cocktail mix (15 mg ml^{-1} and 1 mg ml^{-1}, respectively, in PBS). Anaesthesia was maintained throughout the course of the experiment with vaporized isofluorane delivered by a nose cone as previously described[10]. Image stacks were acquired with a LaVision TriM Scope II (LaVision Biotec) microscope equipped with a tunable Chameleon Ultra (Coherent) Ti:Sapphire laser. To acquire serial optical sections, a laser beam (740 nm for Alexafluor 350; 940 nm for H2BGFP; 1,040 nm for RFP and tdTomato; 990 nm for simultaneous excitation of GFPActin and H2BmCherry) was focused through a ×20 or ×40 water immersion lens (N.A. 1.0 and 1.1 respectively; Zeiss) and scanned with a field of view of 0.5 or 0.25 mm^2, respectively, at 600 Hz. Z-stacks were acquired in 1–3 μm steps to image a total depth of 150 μm of tissue. We revisited the same hair follicles in separate experiments as previously described[10]. For time-lapse recordings, serial optical sections were obtained between 1 to 5 min intervals, depending on the experimental setup. Laser ablation was carried out with the same optics as used for acquisition. An 800 nm laser beam was used to scan the target area (10–50 μm^2) and ablation was achieved using 30–50% laser power for ~1 s. Ablation parameters were adjusted according to the depth of the target (50–100 μm).

Image analysis. Raw image stacks were imported into Fiji (NIH) or Imaris software (Bitplane/Perkin Elmer) for further analysis. Provided images and Supplementary Videos are typically presented as a maximal projection of 3–6 μm optical sections. For visualizing individual labelled cells expressing the tdTomato Cre reporter, the brightness and contrast were adjusted accordingly for the green (GFP) and red (RFP/tdTomato) channels and composite serial image sequences were assembled as previously described. Hair follicle length and labelled cell position values were measured from the top of the stem cell compartment. Apoptotic cell tracking analysis was performed in Imaris software (Bitplane).

Electron microscopy. Trimmed skin samples were fixed (2% gluteraldehyde and 2% paraformaldehyde in 0.1 M sodium cacodylate buffer pH 7.4) for 1 h. The samples were rinsed in sodium cacodylate buffer and were post-fixed in 1% osmium tetroxide for 1 h. The samples were rinsed and en bloc stained in aqueous 2% uranyl acetate for an hour further, followed by rinsing, dehydrating in an ethanol series to 100%, and rinsing several times in 100% propylene. Then samples were infiltrated with Embed 812 (Electron Microscopy Sciences) resin and baked overnight at 60 °C. Hardened blocks were cut using a Leica UltraCut UC7. Sixty-nanometre sections were collected and stained using 2% uranyl acetate and lead citrate for transmission microscopy, and 250-nm-thick sections were stained with either Richardson's stain or 1% Toluidine Blue for light microscopy. For immunolabelled electron microscopy, dissected skin samples were fixed in 4% paraformaldehyde/0.1% gluteraldehyde in phosphate buffer for 30 min and then in 4% paraformaldehyde/phosphate buffer overnight at 4 °C. The samples were rinsed in 0.1 M HEPES. To quench, aldehydes were placed in 50 mM NH_4Cl plus 100 mM glycine plus 2% sucrose for 1 h, then washed in HEPES buffer and placed in 0.1% tannic acid/0.1 M HEPES for 1 h, then rinsed in 50 mM Tris/50 mM maleate and placed in 2% uric acid/50 mM Tris/50 mM maleate for 1 h. After rinsing, they were dehydrated through a graded series 50% to 95% of ethanol at 4 °C, then infiltrated with 50:50 ethanol/LR White (EMS) for 1 h followed by several changes of pure 100% LR White overnight on a rotator at 4 °C. Samples were polymerized at 60 °C for 18 h. Fifty-nanometre resin sections were cut on a Leica UC7 ultra-microtome and collected on nickel formvar/carbon grids, and immunolabelled using a primary chicken anti-GFP (Abcam) diluted to 1:50 for 1 h, rinsed and placed on protein A gold secondary 1:50 (University of Utrecht). The sections were counterstained with 2% uranyl acetate and lead citrate. Grids were viewed FEI Tencai Biotwin TEM at 80 kV. Images were taken using Morada CCD and iTEM (Olympus) software.

Immunostaining on paraffin sections and whole-mount skin. Skin was fixed in 4% PFA for whole mount or in 10% formalin for paraffin embedding and used for histological analysis as previously described[26]. Immunohistochemistry was performed by incubating sections at 4 °C overnight with primary antibodies as follows: mouse anti-β-catenin (1:100, BD #610153; 14/Beta-Catenin), rat anti-CD11b (1:250, eBioscience #14-0112; M1/70), goat anti-P-cadherin (1:100, R&D #AF761), rabbit anti-pSmad2 (Ser465/467) (1:1,000, Cell Signaling #3108; 138D4), and rabbit anti-Lef1 (1:100, Cell Signaling #2286; C18A7). pSmad2 immunostaining required TSA Plus kit (PerkinElmer). For bright-field immunohistochemistry, biotinylated species-specific secondary antibodies, followed by detection using the ABC kit (Vector Labs) and DAB kit (Vector Labs), were used according to the manufacturer's instructions. M.O.M. kit was used for mouse antibodies (Vector Laboratories). Secondary antibodies conjugated with FITC, RRX and Cy5 (Jackson Immunoresearch Laboratories) were used at a concentration of 1:100 for 1 h at room temperature. Alexafluor 350 phalloidin (Life Technologies) was used according to the manufacturer's instructions.

FACS. Back skins of *K14-H2BGFP; Lef1-RFP* and *Lgr5-CreER; Tgfbr1*$^{fl/fl}$ or *Tgfbr1*$^{fl/+}$; *tdTomato*; *K14-H2BGFP* mice were harvested at P12, P16 or P20 and were placed dermis down on 0.2% collagenase (Sigma) at 37 °C for 20 min, and then placed on 0.25% trypsin (Gibco) at 37 °C for 10 min to obtain epithelial cells as previously described[27]. Cells were stained for 10 min with biotinylated rat anti-CD34 (1:50, eBiosciences #14-0341; RAM34), biotinylated rat anti-CD45 (1:50, BD #553077; 30-F11), biotinylated rat anti-CD117 (1:50, BD #553353; 2B8) and goat anti-integrin-α9 (1:50, R&D #AF3827). Cells were washed for 5 min and then incubated with streptavidin-Pacific blue (1:200, Invitrogen) and Alexafluor 647 donkey anti-goat IgG (Jackson Immunoresearch Laboratories). Cells were isolated on DAPI exclusion and by the following criteria: dermal papilla = RFP$^+$, CD34$^-$, CD45$^-$, CD117$^-$, integrin-α9$^+$; and enriched outer root sheath = RFP$^-$, GFP^{High} using a FACSAria II Cell Sorter (BioScience), as previously described[28]. Cells were sorted into RNA lysis buffer for RNA isolation (RNease Mini Kit, Qiagen). FACS profiles were analysed through FlowJo software.

RT–qPCR. cDNA was made using Superscript III First-Strand Synthesis kit (Invitrogen). RT–qPCR was performed in triplicate with SYBER Green I reagents (Invitrogen) using 5.0 ng cDNA per reaction on the ViiATM 7 Real-Time PCR system (Invitrogen, Life Technologies). Data were analysed by ViiATM software, Microsoft Excel and PRISM. Gene-specific primers were designed and are listed in Supplementary Table 1.

Statistical analysis. Data are expressed as percentages, box and whisker plots (error bars represent maximum and minimum), or mean ± s.d. An unpaired Student's *t*-test was used to analyse data sets with two groups and $*P < 0.05$ to $****P < 0.0001$ indicated a significant difference. Statistical calculations were performed using the Prism software package (GraphPad). No statistical method was used to predetermine sample size.

17. Tumbar, T. *et al.* Defining the epithelial stem cell niche in skin. *Science* **303,** 359–363 (2004).
18. Rendl, M., Lewis, L. & Fuchs, E. Molecular dissection of mesenchymal–epithelial interactions in the hair follicle. *PLoS Biol.* **3,** e331 (2005).
19. Vaezi, A., Bauer, C., Vasioukhin, V. & Fuchs, E. Actin cable dynamics and Rho/Rock orchestrate a polarized cytoskeletal architecture in the early steps of assembling a stratified epithelium. *Dev. Cell* **3,** 367–381 (2002).
20. Harada, N. *et al.* Intestinal polyposis in mice with a dominant stable mutation of the β-catenin gene. *EMBO J.* **18,** 5931–5942 (1999).

21. Barker, N. *et al.* Identification of stem cells in small intestine and colon by marker gene *Lgr5*. *Nature* **449,** 1003–1007 (2007).
22. Harfe, B. D. *et al.* Evidence for an expansion-based temporal Shh gradient in specifying vertebrate digit identities. *Cell* **118,** 517–528 (2004).
23. Clausen, B. E., Burkhardt, C., Reith, W., Renkawitz, R. & Förster, I. Conditional gene targeting in macrophages and granulocytes using LysMcre mice. *Transgenic Res.* **8,** 265–277 (1999).
24. Jung, S. *et al.* Analysis of fractalkine receptor CX3CR1 function by targeted deletion and green fluorescent protein reporter gene insertion. *Mol. Cell. Biol.* **20,** 4106–4114 (2000).
25. Madisen, L. *et al.* A robust and high-throughput Cre reporting and characterization system for the whole mouse brain. *Nature Neurosci.* **13,** 133–140 (2010).
26. Zito, G. *et al.* Spontaneous tumour regression in keratoacanthomas is driven by Wnt/retinoic acid signalling cross-talk. *Nature Commun.* **5,** 3543 (2014).
27. Greco, V. *et al.* A two-step mechanism for stem cell activation during hair regeneration. *Cell Stem Cell* **4,** 155–169 (2009).
28. Clavel, C. *et al.* Sox2 in the dermal papilla niche controls hair growth by fine-tuning BMP signaling in differentiating hair shaft progenitors. *Dev. Cell* **23,** 981–994 (2012).